NUCLEAR PHYSICS

Nuclear Reactions with Stable and Radioactive Ion Beams at LAFN-IFUSP

Radioactive Ion Beams in BraSil—RIBRAS Facility

Alinka Lépine-Szily[1] (ORCID)

Abstract

We present an outlook of studies performed in collaboration or inspired by Prof. Mahir Hussein. The first part refers to the elastic scattering measurements performed in the 80–90 with α-structured systems with strong oscillations in the angular distributions and a large increase of the cross-sections at backward angles, an effect called Anomalous Large Angle Scattering (ALAS). The second part refers to the installation of the "Radioactive Ion Beams in BraSil" (RIBRAS) facility, which was an idea promoted by Prof. Hussein and became reality due to his strong support. It was installed in 2004 as the first radioactive ion beam facility in the southern hemisphere and it has been operating continuously since then. In this paper, we will describe the facility, and some interesting results obtained with the 2-neutron-halo, exotic ^{6}He beam, provided by RIBRAS.

Keywords ALAS · Nuclear reactions · Radioactive Ion Beams in Brasil · RIBRAS

1 Introduction

The leitmotiv of this paper is the presentation of measurements and studies we performed in collaboration or inspired by Prof. Hussein. It is divided in two different subjects, which were executed at different times. The first refers to studies dedicated to the Anomalous Large Angle Scattering (ALAS) effect and were executed in the eighties and nineties of the last century; however, there is still work going on on these intriguing effects. Even if tools and means have been found to describe these effects, it seems that the mechanism is depending on the particular system and the comprehension of their origin is still incomplete. The contribution of prof. Hussein to this subject is very important and I wish to show it in this paper.

The beams delivered by the 8 MV Pelletron Tandem installed in the Open Laboratory of Nuclear Physics (LAFN) of the Institute of Physics of the University of São Paulo (IFUSP) allowed to measure the elastic scattering of α-structured ions (^{12}C, ^{16}O) on α-structured targets (^{12}C, ^{24}Mg, and ^{28}Si). Strong oscillations in the angular distributions have been observed with a large increase of the cross-sections at backward angles, an effect called Anomalous Large Angle Scattering (ALAS). This effect had been observed previously [1] and several models proposed for its explanation, as Regge poles with the l-value determined by the period of oscillations, odd-even staggering in the S-matrix, parity-dependent optical potentials, shape-resonances, even compound nuclear fluctuations. These features mobilized a lot of attention and Prof. Hussein was very much interested in these problems. The measured angular distributions and excitation functions were used as benchmark for calculations using different models or reaction mechanisms. Mention to some more recent papers will show that still today the problem is investigated and the contribution of Prof. Hussein can be felt, with numerous citations of his contributions to this field.

The second subject treated is this paper refers to the installation of the Radioactive Ion Beams in BRASil (RIBRAS) facility at LAFN and some interesting results obtained with it. Prof. Hussein was the coordinator of the grant project funded by FAPESP, that made its implementation feasible. The idea became reality in 2004

✉ Alinka Lépine-Szily
alinka@if.usp.br

1   Instituto de Física, Universidade de São Paulo, São Paulo, SP, 05508-090, Brazil

with the "Radioactive Ion Beams in BraSil" (RIBRAS) being the first radioactive ion beam facility in the southern hemisphere. A description of the RIBRAS system is presented in this paper. It is followed by results of elastic scattering measurements using the two-neutron halo nucleus ^{6}He beam on light, medium mass and heavy targets. The data are analyzed using up-to-date methods as Continuum Discretized Coupled Channels (CDCC) calculations.

2 The Anomalous Large Angle Scattering Effect

The ^{24}Mg+^{12}C elastic scattering and the α-transfer reaction ^{24}Mg(^{12}C,^{16}O)^{20}Ne were measured at 40-MeV incident energy. Discussions with Prof. Hussein resulted in assuming that the ALAS effect was produced by the coupling between the elastic scattering and the α-transfer amplitudes. The method to calculate the coupling was developed by W.E. Frahn and Mahir Hussein [2]. Starting from coupled-channel equations, they used suitable approximations to calculate directly the corrections to the elastic partial-wave S-matrix that arise from the feedback of certain strongly coupled channels on elastic scattering. The calculation has shown that the coupling between the α-transfer and elastic channel can account for the intermediate angle oscillations observed in the elastic scattering angular distributions [3].

The same idea of a multistep α-transfer picture was used by Prof. Hussein and his collaborators Luiz Felipe Canto and Raul Donangelo to describe ALAS observed for the ^{16}O+^{28}Si system. The transfer of two and three α-particles was described in a semiclassical treatment of the interplay between absorption and transfer processes. The energy dependence of the contribution to the elastic S-matrix due to these processes was estimated and shown to be consistent with the overall trend of the data [4].

Complete elastic scattering, and some α-transfer angular distributions were measured at many energies for the following systems: ^{16}O + ^{24}Mg [5, 6], ^{12}C + ^{16}O [7], ^{12}C + ^{28}Si [8, 9], ^{16}O + ^{28}Si [10], and ^{12}C+ ^{24}Mg [11–14]. In the case of ^{16}O + ^{24}Mg, both elastic and α-transfer angular distributions and excitation functions had been measured. These data were analyzed in a similar spirit however describing the coupling between the α-transfer and elastic channel through a polarization potential which was able to reproduce the data quite well [5, 6]. Not only the oscillating angular distributions but also the strongly structured excitation functions (see Fig. 1) could be reproduced by the α-transfer mechanism.

Another important insight of Prof. Hussein was the idea that these complete elastic scattering angular distributions could be used for other goals also, such as to obtain information on the total reaction cross-section σ_R or on the
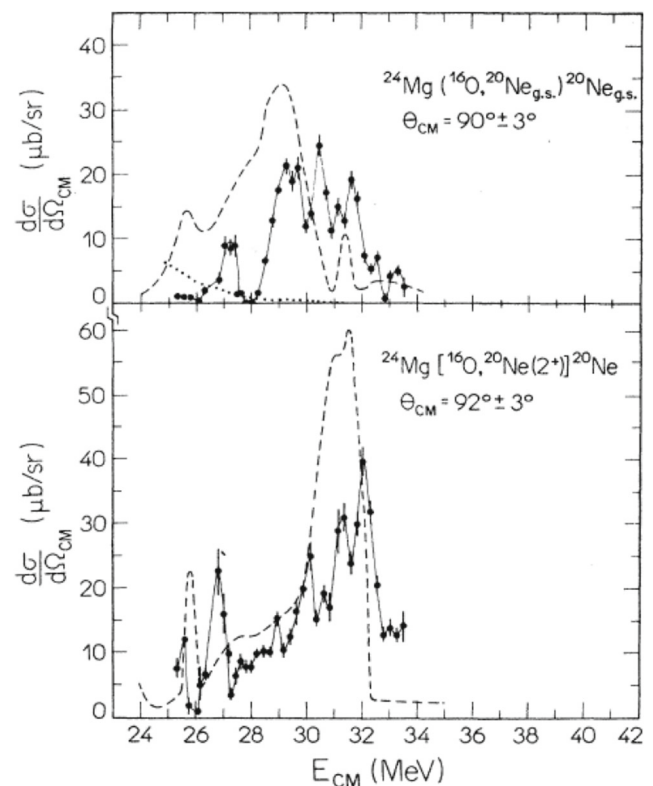
Fig. 1 Excitation functions of the indicated reactions. Solid lines are to guide the eye. The dashed line is the result of calculation with V_{pol} and dotted line without V_{pol}. This figure has been extracted from Ref. [6]

nuclear forward glory amplitude f$_{nucl}$(0) using the Optical Theorem applied to charged particle collisions [15]. Prof. Hussein gave the idea to use the Optical Theorem to obtain the total reaction cross-section from the elastic scattering angular distributions to Antonio Carlos Villari for the final examination in the graduate nuclear physics course. This gave origin to a publication of Villari together with Mahir Hussein and Herch Moyses Nussenzveig [16].

The Optical Theorem relates the imaginary part of the total scattering amplitude at 0° to the total scattering cross-section. Subtracting the Rutherford cross-section from the total cross-section and the Rutherford amplitude from the total scattering amplitude, one arrives at a quantity called $\Delta\sigma_T$, which can be written as:

$$\Delta\sigma_T = \sigma_R - \int d\Omega [\frac{d\sigma_{\text{Ruth}}}{d\Omega} - \frac{d\sigma_{el}}{d\Omega}] \tag{1}$$

where σ_R is the total reaction cross-section, $\frac{d\sigma_{\text{Ruth}}}{d\Omega}$ is the differential Rutherford cross-section and $\frac{d\sigma_{el}}{d\Omega}$ is the differential elastic cross-section.

$\Delta\sigma_T$ can also be written as:

$$\Delta\sigma_T = (\frac{4\pi}{k})Im[f(0) - f_{\text{Ruth}}(0)], \tag{2}$$

where f and f_{Ruth} are the total and Rutherford scattering amplitudes, respectively, and k is the asymptotic wave number of relative motion. The occurrence of nuclear forward glory, a refractive effect, leads to a major enhancement in $\Delta\sigma_T$.

This idea was applied to the ^{12}C + ^{16}O [7], and ^{12}C + ^{28}Si systems [8]. Complete elastic scattering angular distributions were measured at several energies and total reaction cross-sections were deduced as a function of energy for both systems, as well as the nuclear forward glory amplitude [7, 17]. The available elastic scattering data on the ^{12}C + ^{12}C system was used to obtain the $\Delta\sigma_T$, related to the nuclear forward glory amplitude $f_N(0)$, to compare different nuclear interactions for this system [18].

The hypothesis that the ALAS effect was related to the coupling between the elastic and α-transfer channels, gave origin to new calculations, using new tools. Invited by Prof. Hussein, Franco Iachello visited our Institute and gave a series of lectures on his Algebraic Scattering Theory. At the time of his visit, Iachello was interested in using his algebraic methods in scattering problems, that is, determining solutions in the continuum instead of the bound states. Iachello and his collaborators were working on the problem of identifying dynamic symmetries in scattering problems and constructing scattering matrices, S, from the dynamic group. In this way, one could obtain cross-sections directly from the S matrix, without solving the Schrödinger equation. The first example was the non-relativistic scattering by a Coulomb potential [19], which is exactly related with the symmetry group SO(3,1). They

found that all problems with SO(3,1) symmetry imply S matrices which for partial wave l and momentum k, have the form:

$$S_l(k) = \frac{\Gamma(l + 1 + iv)}{\Gamma(l + 1 - iv)} \tag{3}$$

The actual value of v depends on the explicit expression for the Hamiltonian H. For the Coulomb problem, one obtains $v(k) = \mu Z_1 Z_2 e^2/\hbar^2 k$, where μ is the reduced mass and Z_1, Z_2 are the charges of the colliding particles. In the case of heavy-ion reactions at low energies, v will be represented by a complex nuclear part summed to the above Coulomb term. In analogy with $V(r)$ in the Schrödinger equation, the v term is called an "algebraic potential." The main advantage of the algebraic description appears when one has many outgoing channels, such as elastic scattering, inelastic scattering to several excited states and transfer reactions to several final states. In the "Algebraic Scattering Theory" (AST), one has a set of coupled algebraic equations, much easier to solve than the set of coupled differential Schrödinger equations.

Six channels of the ^{12}C+^{24}Mg system have been measured at 40 MeV: the elastic scattering, the inelastic scattering leading to the first, the second + third excited states of ^{24}Mg, and the α-transfer reaction leading to the ground state, first and second excited states of ^{20}Ne. All angular distributions were strongly oscillating and with a large increase in the cross-section at backward angles, a typical ALAS feature. The AST was used to couple the seven channels. Without any coupling,

Fig. 2 Experimental angular distributions of the indicated reactions. The solid lines are the result of the calculations coupling seven reactions channels in the AST scheme. Taken from Ref. [20]
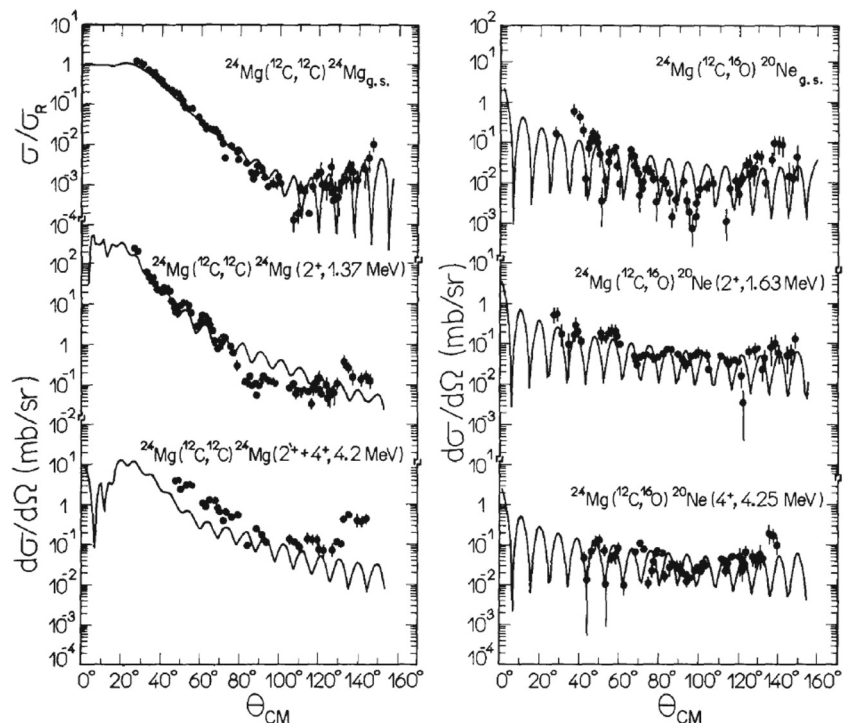
the calculated elastic channel cross-section σ/σ_R had the typical exponential decrease with increasing angle, not presenting the ALAS effect. When including the coupling to the inelastic channels, the effect was small at backward angles. Including, one by one, the transfer channels, the effect increased, yielding a perfect fit with all seven couplings. We present in Fig. 2 the results of this calculation. All angular distributions were well reproduced by these calculations [20]. The AST was also applied to calculate the orbiting effect observed in the collision between the ^{18}O beam and the ^{10,11}B targets [21]. We coupled 22 inelastic and transfer channels, and could reproduce the observed $1/\sin\theta_{c.m.}$ angular distributions of the Q-value integrated cross-sections. The experimental Q-value integrated differential cross-sections were obtained by summing over all angular distributions of inelastic and transfer channels, respectively. We concluded that the back-angle anomaly (ALAS) and the orbiting are related phenomena and both can be explained by the strong coupling to transfer channels.

More recently for some light systems without α structure, as, e.g., ^{7}Li+^{14}N [22] and ^{9}Be+^{11}B [23] have also shown the ALAS effect and the data were compared to Coupled Reaction Channel (CRC) calculations with the coupling of a large number of inelastic and transfer channels. Differently from the α structured systems, here the largest effect was due to the reorientation of the colliding partners.

Recently the fifteen strongly oscillating angular distributions of the elastic scattering of ^{12}C + ^{24}Mg [12] at energies around the Coulomb barrier ($E_{c.m.} = 10.67 - 16.00$ MeV) were revisited and reproduced by adding five Breit-Wigner resonance terms to the l = 2,4,6,7,8$\hbar$ elastic S matrix terms [14]. The nonresonant, background elastic scattering S matrix is calculated using a microscopic double folding potential, also called the São Paulo Potential [24, 25]. The J = 2,4,6,7,8$\hbar$ molecular resonances fit well into a rotational molecular band, together with other higher lying resonances observed in the ^{16}O + ^{20}Ne elastic scattering. It was proposed that the presently observed, largely deformed molecular band corresponds to the hyperdeformed band in ^{36}Ar compound nucleus, which has been found previously in α-cluster calculations, as well as in a new Nilsson model calculation [26].

To conclude, we can say that the phenomenon of ALAS is still being investigated in elastic scattering of α-multiple nuclei or nuclei with one α particle as cluster [14, 27]. In nowadays, microscopic double folding models have been used to construct a potential for use in scattering problems and more powerful approaches such as coupled reaction calculation (CRC) and cluster folding model [14, 23, 27, 28] have been used. The contribution of Prof. Hussein in the field can still be felt.

3 Radioactive Ion Beams in BraSil

The development of radioactive beams can help in the quest of full understanding of the collective and single particle aspects and their correlations in complex nuclei. They permit an expansion from the one dimensional image with the variation of the nuclear mass A, to a two-dimensional one, with the existence of a large number of bound, however unstable isobars, where the proton number Z as well as the neutron number $A–Z$ can vary over a wide range. Many kinds of new phenomena are present in the unstable nuclei: for instance, very neutron rich nuclei allow the study of unusual properties of weakly bound quantum systems, such as the nuclear halo [29, 30]. In halo nuclei, the wave function of the last neutrons with low orbital momenta (l = 0,1), can extend to large distances from the core. Nuclei far from the stability line also present changes in the shell structure, with new magic numbers [31, 32].

Radioactive ion beams (RIB) can be produced by several reaction mechanisms [33]. The most important are the in-flight fragmentation of the projectile, and the spallation or target fragmentation followed by the isotope separation online (ISOL) method. These processes occur at intermediate and high incident energies and are used at many large laboratories around the world. They have the advantages such as high intensity, can produce light and heavy radioactive beams, and the possibility to move further away from the stability valley. At much lower energies, transfer reactions, fusion, or even fission can produce RIB and, in this way, small laboratories with quite low energy accelerators are also making important contributions in this field. There are problems that are more advantageous to be observed at energies close to the Coulomb barrier, such as reaction mechanisms involving exotic light nuclei, in particular, the effect of halo on nuclear reactions, reactions of astrophysical interest, sub-barrier fusion, and many other examples. On the other hand, many low energy accelerators have been closed and funding channeled to laboratories with much higher energy.

The idea of installing a radioactive ion beam facility in LAFN was born in 1997 in a workshop organized by Prof. Hussein. He became the coordinator of the grant project funded by FAPESP, that made its implementation feasible. The idea became reality in 2004 with the "Radioactive Ion Beams in BraSil" (RIBRAS) beginning its operation. In Fig. 3, we present the RIBRAS system [35–37] installed on the beam line at 45° in the experimental hall B of LAFN. The RIBRAS system consists of two superconducting solenoids and uses the "in-flight method" to produce radioactive ion beams using the primary beam provided by the 8UD Pelletron Tandem of IFUSP . The choice for a solenoid-based system was motivated by the successful

Fig. 3 Photo of the RIBRAS system. Taken from Ref. [34]

example of the TWINSOL facility [38] installed in the Nuclear Physics Laboratory of the Notre Dame University.

The RIBRAS system consists of two large air-core (30-cm clear warm bore) superconducting solenoids with 6.5-T maximum central field (5-Tm axial field integral). The superconducting solenoids were manufactured by Cryomagnetics Inc. (USA). The magnet coils are immersed in a liquid helium (LHe) dewar which contains a maximum of 250 l of LHe, with a boil-off rate of 2–3 l/day. Around the LHe vessel, a liquid nitrogen vessel of 130 l and vacuum shields are localized to minimize the LHe consumption. A recovery system collects the helium gas evaporating from the dewars and is liquefied at IFUSP. In Fig. 4, a schematic

view of the system is presented. The production system (primary target) consists of a gas cell, mounted in chamber-1, before the first solenoid. The primary target can be a gas or a solid target, such as a ^{9}Be foil, which is mounted as the gas cell window. After the gas cell, downstream in the beam line, there is a tungsten rod with electron suppression and with a cylindrical hole (geometrical suppression) to stop and collect the primary beam particles (Faraday cup). The maximum angular acceptance is limited to 6° by a collimator located at the entrance of the first solenoid. The angular divergence of the secondary beams entering the first solenoid is 4°, between 2 and 6°, in this setup. The angular divergence of the secondary beam in chamber-2,
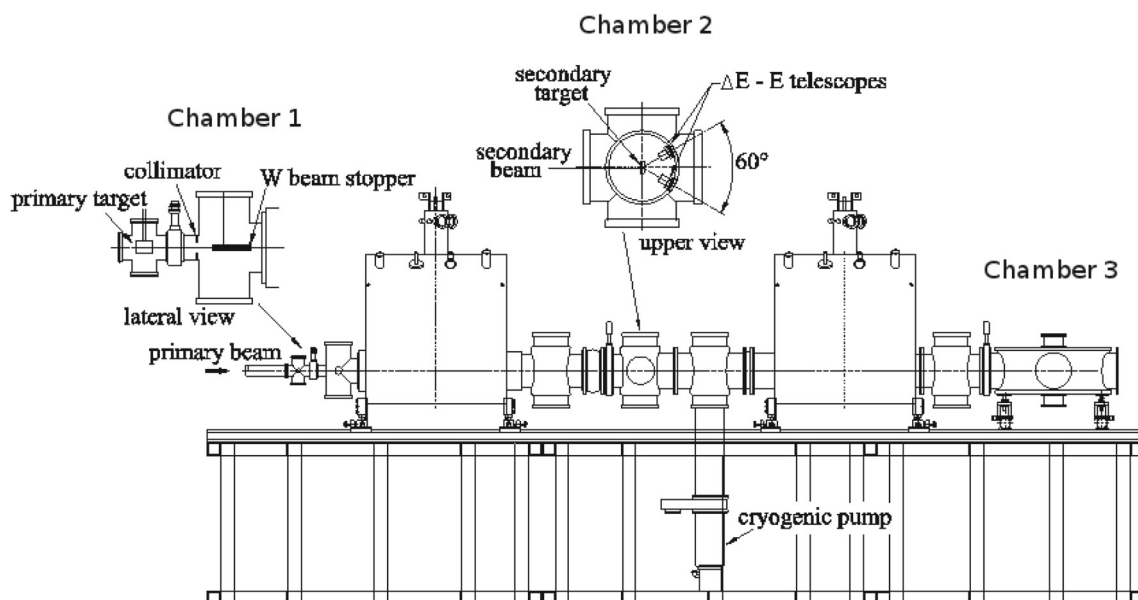
Fig. 4 The experimental setup of RIBRAS: the stable beam comes from the left, the production target, located in chamber-1 is followed by the W beam stopper and the first solenoid, which is followed by the

central scattering chamber-2, with the secondary target and detectors installed in it, followed by the second solenoid and the large scattering chamber-3. Taken from Ref. [39]

after the first solenoid, is 3.2°, between 1.3 and 4.5°. The reaction products, which emerge from the primary target in the forward angle region and go through the first solenoid, are selected and focused by their magnetic rigidity. As the first magnet focuses all ions with the same magnetic rigidity, i.e., the same ME/Q^2 ratio, where M, E, and Q stand for mass, energy, and charge state of the ion, the beam of interest can be accompanied by contaminant beams of the same magnetic rigidity, but with different charges, masses and energies. The transmission of the beam of interest to chamber-2 is optimized by varying the current of the first solenoid and maximizing the intensity of the beam of interest detected in a $\Delta E - E$ Si telescope after its elastic scattering on a ^{197}Au target mounted in chamber-2. The radioactive beam of interest can be cleaned after the second solenoid by passing through a degrader mounted in chamber-2, which changes the magnetic rigidity of the beam of interest and contaminant beams by different amounts, since the energy loss in the degrader depends on MZ^2/E.

The transfer reactions are the best options to produce radioactive nuclear beams using primary beams at energies provided by the LAFN Pelletron accelerator. As examples, the one-nucleon transfer reactions which are used to produce reasonably intense beams of ^{8}Li and ^{6}He, (respectively 10^6 pps and 10^5 pps for 1μA primary beam), are ^{9}Be (^{7}Li, ^{8}Li) ^{8}Be and ^{9}Be (^{7}Li, ^{6}He) ^{10}B. However, to produce the exotic, proton-halo ^{8}B beam, it is necessary to use a two-proton transfer reaction, such as ^{3}He (^{6}Li, ^{8}B) n, where a ^{3}He gas cell is required and a lower intensity is obtained (10^4 pps per 1-μA primary beam).

The ion beams produced so far by RIBRAS are ^{6}He, ^{8}Li, ^{7}Be, ^{10}Be, ^{8}B, and ^{12}B with intensities that can vary from 10^4 to 10^6 pps. ^{6}He and ^{8}B, are halo nuclei, respectively, with a 2 neutron halo and a 1 proton halo. These halo nuclei are often called "exotic" nuclei because the very low binding energy of the halo nucleons and their large extension can give origin to new phenomena. In the of 15 years of RIBRAS operation, dozens of Masters degree and PhD degree studies were executed using the radioactive beams of the RIBRAS system. The number of publications in refereed journals or refereed conference proceedings on measurements executed using the RIBRAS system is 56. The main users are researchers from IFUSP and from other Brazilian institutions but we also have external visitors. Many post-doctoral fellows, also from abroad, have profited from the installations.

4 Elastic Scattering of ^{6}He 2n-halo Nucleus on ^{9}Be, ^{27}Al, ^{58}Ni, and ^{120}Sn Targets

Initially, when only the first solenoid was used, the secondary beams were not pure. For this reason, most early experiments performed at RIBRAS were on elastic scattering. Elastic angular distributions were measured for the available radioactive beams, such as ^{6}He [39–42], ^{8}B [43] , ^{8}Li [44–46], ^{7,10}Be [47, 48], and ^{12}B [49] on light, medium mass, and heavy targets at various energies, near and above the Coulomb barrier. The presence of many α-particles observed with the ^{6}He beam was the subject of several studies [50, 51]. Their origin is still controversial; transfer reactions or breakup is the possible explanation. These measurements are important since they determine the optical potentials between the radioactive projectiles and the targets. These can be quite different from those of stable systems due to the halo structure or the low binding energy of the radioactive nuclei. The elastic scattering also gives information on the total reaction cross-section and on the size of the nuclei involved. The coupling of the elastic scattering to other important channels, such as breakup or transfer, strongly enhanced with radioactive projectiles, can also be investigated through the elastic scattering experiments.

4.1 ^{6}He + ^{9}Be Elastic Scattering

Elastic scattering angular distributions were measured at energies E_{lab} = 16.2 and 21.3 MeV of the ^{6}He beam scattered on a ^{9}Be target mounted on a target tower in the center of the scattering chamber-2. Four $\Delta E - E$ Si telescopes mounted on a rotating plate detected the scattered particles [40]. The absolute normalization of the measurements is obtained by alternating successively the ^{9}Be target with a gold target, where the energies are well below the Coulomb barrier and the scattering is pure Rutherford scattering. Besides the elastic data, the experiment showed a large yield of α-particles, presumably coming from the projectile breakup or neutron-transfer to target states or even from the target breakup, since both projectile and target nucleus are weakly bound, respectively, by 0.973 MeV and 1.665 MeV for ^{6}He and ^{9}Be.
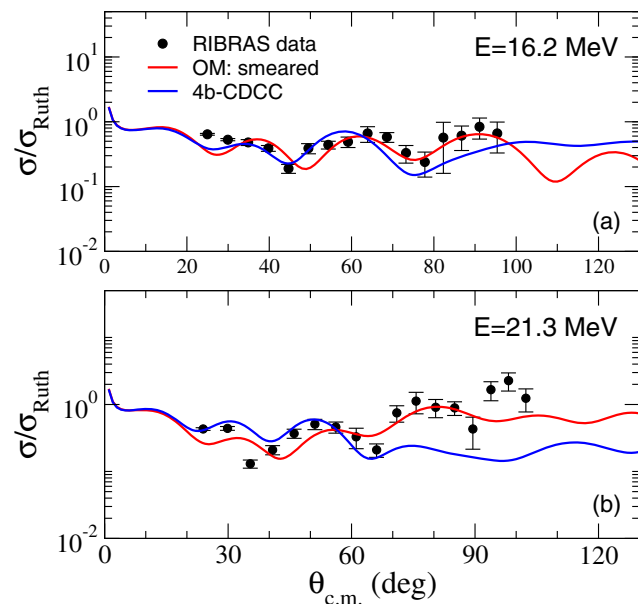
The Coulomb barrier of the ^{6}He + ^{9}Be system is V_{CB}(lab) = 2.2 MeV, and thus the beam energies are well above the Coulomb barrier. It means that, for these data, the Coulomb interaction is not important and we observe a diffraction pattern of Fraunhofer type rather than the Fresnel type observed so far for heavier systems. The elastic scattering cross-section can be affected by the projectile breakup and the coupling between the elastic and breakup channel can be calculated by a method called Continuum-Discretized Coupled-Channels (CDCC) [52] method. It is to be noted that, in this description, the forces between the target (T) and different particles of the projectile (n and ^{4}He) provide a mechanism to excite the projectile from the ground state to continuum states. In addition, the interactions U_{n-T} and $U_{^4\text{He}-T}$ are fitted on

elastic scattering data between a neutron and the target $(n - T)$ and ^{4}He-particles and the target (^{4}He-T). Due to this, there are no free parameters in the model and the calculated cross-sections are not a fit to the data but a prediction. The good agreement of the CDCC calculations with experimental elastic scattering data attests its value.

The CDCC calculation assumes that the target stays in its ground state and only the projectile is excited or suffers breakup. This is an approximation for the scattering phenomenon, it provides a satisfactory description of the elastic scattering cross-sections, but usually underestimates the breakup cross-section. The ^{6}He + ^{9}Be elastic scattering data, presented in Fig. 5, are compared to a 4-body CDCC calculations. In the 4-body version, the target interacts with ^{6}He described as a ^{4}He core + 2 neutrons taken into account separately. The agreement is good. In the optical model calculation [53], the projectile-target optical potential was calculated in a cluster model where the contributions from the fragment-target and the dineutron-target are separated and the latter was searched to reproduce the experimental data. The optical model calculation was convoluted by the experimental angular resolution, attenuating the oscillations.

4.2 ^{6}He + ^{27}Al Elastic Scattering

This was the first experiment performed with RIBRAS in 2004. The elastic scattering of the radioactive halo nucleus ^{6}He on ^{27}Al target was measured at four energies, $E_{lab} =$
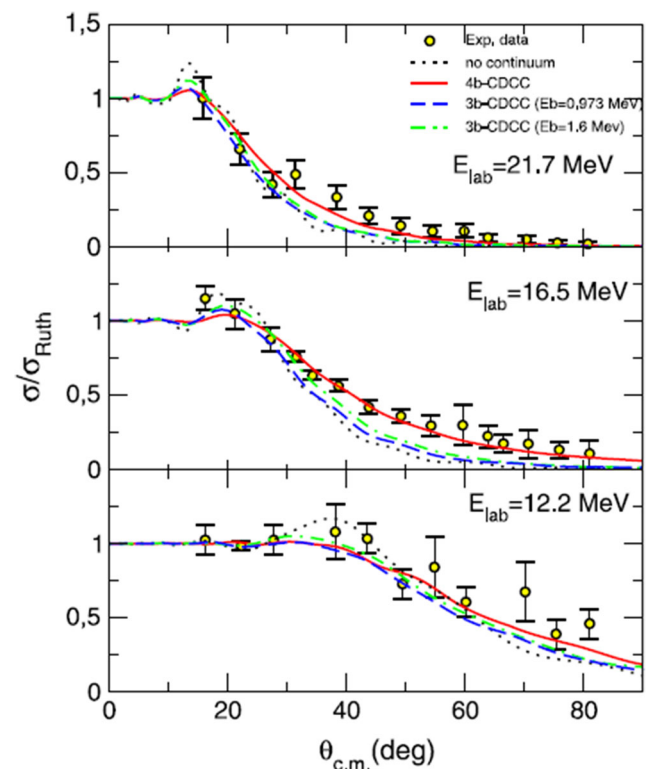
9.5, 11.0, 12.0, 13.4 MeV, close to the Coulomb barrier [39]. The elastic scattering cross-sections of the angular distributions were reproduced by optical model calculations obtained with the São Paulo Potential (SPP) [24, 25], which is a microscopic folding optical potential that takes non-local effects into account. The imaginary part of the potential has the same form factor as the real part and the only free parameters were the normalization of the imaginary potential, N_I and a, the diffuseness of the nuclear density of the projectile.

4.3 ^{6}He + ^{58}Ni Elastic Scattering

The angular distributions of the ^{6}He + ^{58}Ni elastic scattering [41] were measured at bombarding energies above the Coulomb barrier, $E_{lab} = 12.2$ MeV, 16.5 MeV, and 21.7 MeV in scattering chamber-2, with the same experimental setup as described previously. The angular distributions have been analyzed in terms of three- and four-body CDCC calculations considering the effect of the ^{6}He breakup. In Fig. 6, the CDCC calculations are compared with the experimental results. The dotted black line is the 4-body CDCC without coupling to the continuum. The solid red line corresponds to the full 4-body CDCC calculation. The

Fig. 5 The elastic scattering angular distributions of ^{6}He on ^{9}Be measured at $E_{lab} = 16.2$ and 21.3 MeV are represented by black dots. They are compared to 4-body CDCC (blue solid line) [40] and to optical model calculations (red solid line) [53]. Taken from Ref. [40, 53]. Details in the text

Fig. 6 The elastic scattering angular distributions of ^{6}He on ^{58}Ni are compared to 3-body and 4-body CDCC calculations. Taken from Ref. [41]. Details in the text

dashed blue and dash-dotted green lines are the 3-body calculations with 0.973-MeV and 1.6-MeV two-neutron separation energies, respectively. In the 3-body model, the ^{6}He structure is simplified to an alpha-particle core plus a di-neutron which means that the neutron pair is treated as a single particle bound to the alpha core by 0.973 MeV. In an application of the 3-body model to ^{6}He+^{209}Bi scattering [54], it was found that 3b-CDCC was unable to reproduce the angular distributions between 50 and 100°. More recently, an improved 3b-CDCC model was proposed by A. M. Moro [55] which greatly improved the situation. Moro et al. demonstrated that the use of a different separation energy for ^{6}He, 1.6 MeV instead of 0.973 MeV, which reproduces the rms radius of ^{6}He, provided results closer to the 4-body calculations. We can see from Fig. 6 that the effect of coupling to the breakup channel is clearly the flux removal from the forward angles region, reducing the elastic cross-section in the region of the Fresnel peak. This behavior is well reproduced by the three- and four- body models used here. At large angles, however, we observe that the fall of the angular distribution is less steep than expected by the three-body calculations which fail to reproduce the data in this angular region. The behavior in the cross-section at large angles was reproduced only by the four-body CDCC calculation, which gave an excellent agreement.

4.4 ^{6}He + ^{120}Sn

The angular distributions of the ^{6}He + ^{120}Sn elastic scattering were measured at four bombarding energies above the Coulomb barrier, $E_{\mathrm{lab}} = 17.4$ MeV, 18.05 MeV, 19.8, and 20.5 MeV, of the ^{6}He beam scattered on a ^{120}Sn target [42] using the same experimental setup in

chamber-2 such as described previously. Besides the elastic data, the experiment showed the presence of α-particles, presumably coming from the projectile breakup or neutron-transfer to target states [50, 51]. The angular distributions have been analyzed in terms of optical model (OM), three- and four-body CDCC calculations considering the effect of the ^{6}He breakup. The optical potential was Woods-Saxon type and presented the breakup threshold anomaly in its dispersion relation between real and imaginary parts of the potential. In Fig. 7, the experimental results are compared with OM (dashed lines), three-body CDCC(dotted lines), and four-body CDCC (solid lines) calculations. The 3-body calculations used 1.6-MeV two-neutron separation energy. The 3 and 4 body CDCC calculations are similar and reproduce well the experimental data.
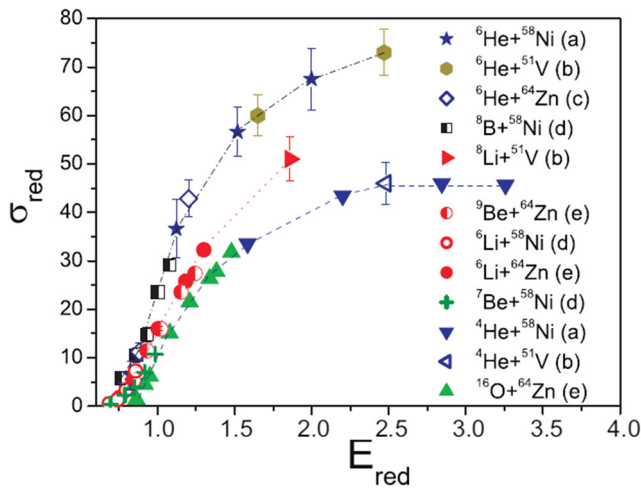
5 Total Reaction Cross-sections

The total reaction cross-section can be deduced from elastic scattering angular distributions, and the optical model or CDCC calculations give the values of total reaction cross-section related to the calculated elastic scattering. To compare the reaction cross-section of different systems at different energies, we make the transformations [56] $\sigma_{\mathrm{red}} = \sigma_{\mathrm{reac}}/(A_p^{1/3} + A_t^{1/3})^2$ and $E_{\mathrm{red}} = E_{\mathrm{cm}}(A_p^{1/3} + A_t^{1/3})/Z_p Z_t$, where $Z_p(Z_t)$ and $A_p(A_t)$ are the charge and mass of the projectile (target), respectively, and σ_{reac} is the total reaction cross-section measured for the system. This procedure accounts for the geometrical effect in the cross-section due to the size of the system and the effect of the Coulomb barrier with respect to the energy. The increase of the reaction cross-sections of weakly bound projectiles, due

Fig. 7 The elastic scattering angular distributions of ^{6}He on ^{120}Sn are compared with OM (dashed lines), three-body CDCC(dotted lines), and four-body CDCC (solid lines) calculations. Taken from Ref. [42]. See text for details
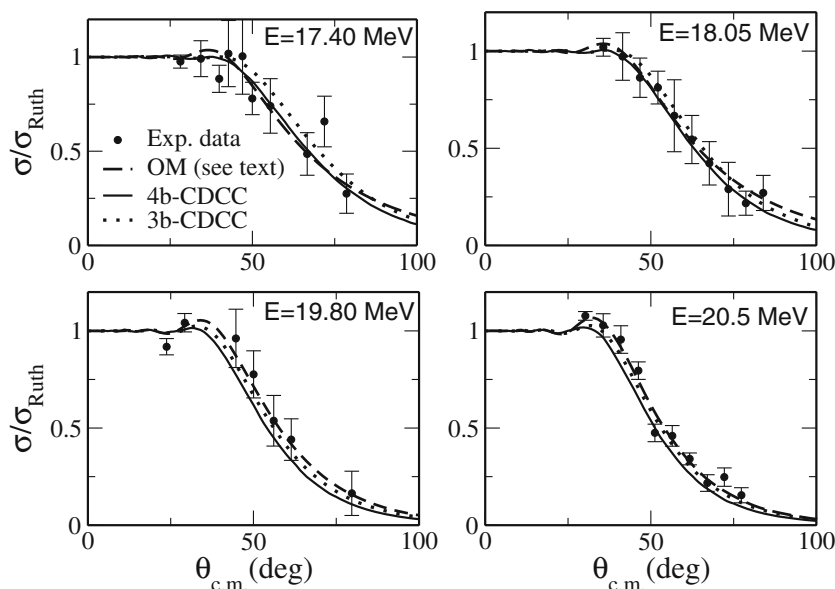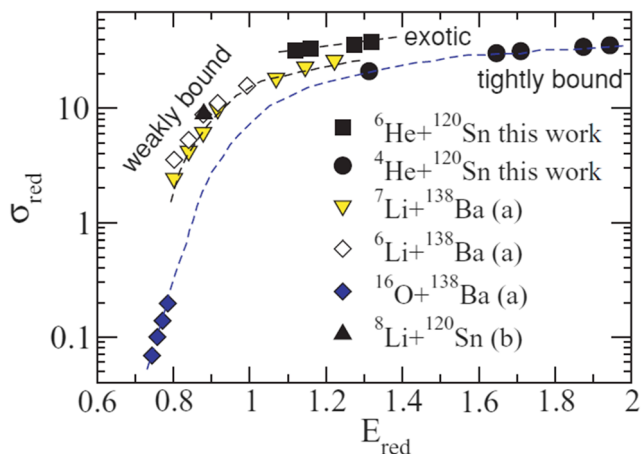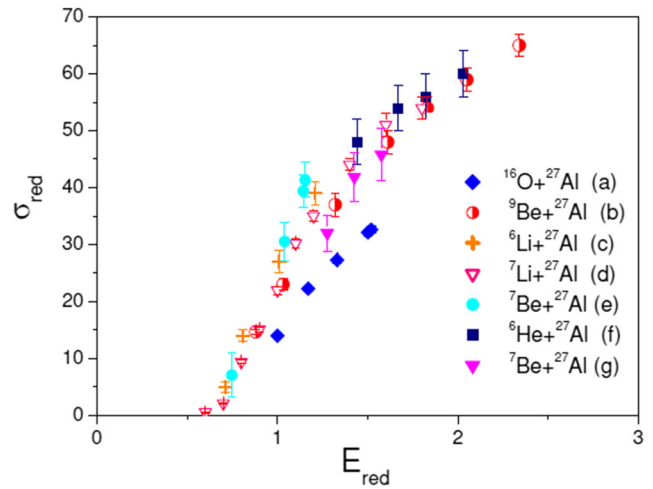
Fig. 8 The reduced reaction cross-section of ^{6}He on ^{58}Ni is presented with other systems of similar masses, as a function of reduced energy. Taken from Ref. [36]. Details in the text

Fig. 10 The reduced reaction cross-section of ^{6}He on ^{27}Al is presented with other systems of similar masses, as a function of reduced energy. Taken from Ref. [48]. Details in the text

either to a fit of the elastic scattering angular distributions or by explicit consideration of the projectile breakup process in the case of a CDCC calculation, is expressed in σ_{reac} and σ_{red} and is not removed by the scaling. On the other hand, the possible lowering of the Coulomb barrier due to the increase in the radius of weakly bound projectiles is not washed out by this scaling. In Figs. 8, 9, and 10, we present reduced reaction cross-sections for targets with mass $A \sim 60$, $A \sim 120$, and A=27, respectively, with projectiles, which are tightly bound (^{4}He, ^{16}O), weakly-bound, stable (^{6,7}Li, ^{9}Be), radioactive (^{7}Be, ^{8}Li), and exotic halo nuclei (^{6}He, ^{8}B). In Fig. 8, we see three bands, the lowest band corresponding to the tightly bound projectiles where the number of open reaction channels is small. For systems with weakly bound projectiles, stable or radioactive, such as ^{6,7}Li, ^{9}Be, and ^{7}Be, ^{8}Li, respectively, the situation changes.

Fig. 9 The reduced reaction cross-section of ^{6}He on ^{120}Sn is presented with other systems of similar masses, as a function of reduced energy. Taken from Ref. [42]. Details in the text

The binding energies of these projectiles are much smaller, respectively, 1.47, 2.46, 1.66, 1.58, and 2.03 MeV and their cluster structure favors the occurrence of transfer reactions. Finally, for the exotic ^{6}He and ^{8}B projectiles, the separation energies (^{6}He→ α+2n) and (^{8}B→^{7}Be+p) are even smaller (0.973 MeV and 0.1375 MeV), respectively, and the halo favors the occurrence of breakup and neutron/proton transfer reactions, which increase even more the total reaction cross-section obtained from CDCC. The same separation in three bands can be observed in Fig. 9. The reaction cross-sections were obtained from the CDCC calculations. The enhancement between reaction cross-sections of radioactive, halo projectiles, when compared to stable, weakly bound projectiles is about 50% for heavy targets at E_{red} = 1.2 MeV , and about 45–50% for the medium mass nuclei at the same reduced energy. Thus, the enhancement, mainly due to the coupling to Coulomb break up, is about the same for medium mass and for heavy targets.

The situation changes for the lighter target A = 27, represented in Fig.10. For the exotic, 2n-halo ^{6}He [39], no important enhancement is seen with respect to weakly bound ^{6,7}Li and ^{9}Be systems; however, all weakly bound (stable or radioactive-halo nuclei) projectiles present a larger reduced reaction cross-section than those for the tightly bound ^{16}O projectile. For all systems, the total reaction cross-sections have been obtained from optical model calculations using the São Paulo Potential. Probably, CDCC calculations should be more adequate for the ^{6}He+^{27}Al system, since it is known that the coupling to the breakup is very important and should be taken into account. On the other hand, the Coulomb breakup should be less important in the case of the ^{27}Al (Z = 13) target than for the systems previously discussed of $A \approx 60$ ($Z \approx 30$) or

$A \approx 120$ ($Z \approx 50$), respectively, where the presence of the halo increased considerably the reaction cross-section. The reduced reaction cross-section for the ^{6}He + ^{9}Be system [53] is $\sim 25\%$ higher than for the weakly bound stable projectiles. There seems to be a minimum in enhancement for the $A = 27$ system, which should be further investigated.

6 Conclusions

We presented several measurements realized in LAFN with stable beams on the ALAS effect with different theoretical interpretations inspired by Prof. Mahir Hussein. The RIBRAS system is described in the sequence with some results obtained with the 2n-halo, exotic beam ^{6}He on light, medium mass, and heavy targets. The elastic scattering cross-sections are reproduced by CDCC calculations, which include the coupling to the breakup. The total reaction cross-sections obtained with the exotic ^{6}He beam are compared with other projectiles, showing a strong enhancement for medium mass and heavy targets due to the Coulomb breakup.

References

1. P. Braun-Munzinger, J. Barrette, Phys. Rep. **87**, 209 (1982)
2. W.E. Frahn, M.S. Hussein, Nucl. Phys. A **346**, 237 (1980)
3. R. Lichtenthaler Jr., A. Lepine-Szily, A.C.C. Villari, et al., Phys. Rev. C **26**, 2487 (1982)
4. L.F. Canto, R. Donangelo, M.S. Hussein, A. Lepine-Szily, Phys. Rev. Lett. **51**, 95 (1983)
5. R. Lichtenthaler Filho, A. Lepine-Szily, A.C.C. Villari, et al., Phys. Rev. C **39**, 884 (1989)
6. A. Lépine-Szily, R. Lichtenthaler Filho, M.M. Obuti, et al., Phys. Rev. C **40**, 681 (1989)
7. A.C.C. Villari, A. Lepine-Szily, R. Lichtenthaler Filho, et al., Nuc. Phys. A **501**, 605 (1989)
8. J.M. de Oliveira Jr., Masters Thesis Institute of Physics of University of Sao Paulo (1988)
9. E.A. Benjamim, A. Lepine-Szily, J.M. Oliveira Jr., et al., J. Phys. Conf. Ser. **436**, UNSP 012015 (2013)
10. J.M. Oliveira Jr., A. Lépine-Szily, A.C.C. Villari, et al., Phys. Rev. C **53**, 2926 (1996)
11. A. Lepine-Szily, W. Sciani, Y.K. Watari, W. Mittig, et al., Phys. Lett. B **304**, 45 (1993)
12. W. Sciani, A. Lepine-Szily, et al., Nuc. Phys. A **620**, 91 (1997)
13. A. Lepine-Szily, M.S. Hussein, R. Lichtenthaler, et al., Phys. Rev. Lett. **82**, 3972 (1999)
14. W. Sciani, Y. Otani, A. Lepine-Szily, et al., Phys. Rev. C **80**, 034319 (2009)
15. J.T. Holdemann, R.M. Thaler, Phys. Rev. **B139**, 1186 (1965)
16. M.S. Hussein, H.M. Nussenzveig, A.C.C. Villari, J.L. Cardoso Jr., Phys. Lett. B **114**, 1 (1982)
17. A.C.C. Villari, F.I.A. Almeida, A. Lepine-Szily, Phys. Lett. B **165**, 247 (1985)
18. M.S. Hussein, A. Lepine-Szily, M.M. Saad, A.C.C. Villari, Phys. Rev Lett. **52**, 511 (1984)
19. Y. Alhassid, F. Iachello, Nuc. Phys. A **501**, 585 (1989)
20. A. Lepine-Szily, MM. Obuti, R. Lichtenthaler Filho, et al., Phys. Lett. B **243**, 23 (1990)
21. A. Lepine-Szily, J.M. Oliveira Jr., P. Fachini, R. Lichtenthaler Filho, et al., Nuc. Phys. A **539**, 487 (1992)
22. A.T. Rudchik, et al., Nuc. Phys. A **700**, 25 (2002)
23. A.T. Rudchik, et al., Nuc. Phys. A **174**, 391 (2003)
24. L.C. Chamon, et al., Phys. Rev. C **66**, 014610 (2002)
25. M.A.G. Alvarez, et al., Nucl. Phys. A **723**, 93 (2003)
26. J. Cseh, J. Darai, W. Sciani, et al., Phys. Rev. C **80**, 034320 (2009)
27. Y. Hirabayashi, S. Ohkubo, Phys.Rev. C **88**, 014314 (2013)
28. N.T.T. Phuc, R.S. Macintosh, N.H. Phuc, D.T. Khoa, Phys. Rev. C **100**, 054615 (2019)
29. I. Tanihata, H. Hamagaki, O. Hashimoto, et al., Phys. Rev. Lett. **55**, 2676 (1985)
30. P.G. Hansen, A.S. Jensen, B. Jonson, Nuclear Halos Annu. Rev. Nucl. Part. Sci. **45**, 591 (1995)
31. T. Otsuka, R. Fujimoto, Y. Utsuno, et al., Phys. Rev. Lett. **87**, 082502 (2001)
32. T. Otsuka, T. Suzuki, R. Fujimoto, H. Grawe, Y. Akaishi, Phys. Rev. Lett. **95**, 232502 (2005)
33. H. Geissel, G. Munzenberg, K. Riisager, Annu. Rev. Nucl. Sci. **45**, 163 (1995)
34. R. Lichtenthaler, et al., AIP Conf. Proc. **1529**, 197 (2013)
35. R. Lichtenthaler, A. Lepine-Szily, V. Guimaraes, C. Perego, et al., Eur. Phys. J. A **25**, 733 (2005)
36. A. Lepine-Szily, R. Lichtenthaler, V. Guimaraes, Eur. Phys. J A **50**, 128 (2014)
37. R. Lichtenthaler, M.A.G. Alvarez, A. Lepine-Szily, et al., Few-Body Syst. **57**, 157 (2016)
38. F.D. Becchetti, J.J. Kolata, the TwinSol Collaboration, Nucl. Instr. Meth. B **376**, 397 (2016)
39. E.A. Benjamim, A. Lépine-Szily, D.R. Mendes Jr., et al., Phys. Lett. B **647**, 30 (2007)
40. K.C.C. Pires, R. Lichtenthaler, A. Lepine-Szily, et al., Phys. Rev. C **83**, 064603 (2011)
41. V. Morcelle, K.C.C. Pires, M. Rodriguez-Gallardo, R. Lichtenthaler, et al., Phys. Lett. B **732**, 228 (2014)
42. P.N. de Faria, R. Lichtenthaler, K.C.C. Pires, A.M. Moro, et al., Phys. Rev. C **81**, 044605 (2010)
43. V. Morcelle, R. Lichtenthaler, A. Lepine-Szily, et al., Phys. Rev. C **95**, 014615 (2017)
44. A. Barioni, V. Guimaraes, A. Lepine-Szily, et al., Phys. Rev. C **80**, 034617 (2009)
45. D.R. Mendes Jr., A. Lepine-Szily, P. Descouvemont, R. Lichtenthaler, et al., Phys. Rev. C **86**, 064321 (2012). Phys. Rev.C **98**, 069901(E)(2018)
46. E. Leistenschneider, A. Lepine-Szily, M.A.G. Alvarez, et al., Phys. Rev.C **98**, 064601 (2018)
47. J.C. Zamora, V. Guimaraes, A. Barioni, et al., Phys. Rev. C **84**, 034611 (2011)
48. V. Morcelle, R. Lichtenthaler, R. Linares, et al., Phys. Rev. C **89**, 044611 (2014)
49. E.O.N. Zevallos, V. Guimaraes, E.N. Cardozo, et al., Phys. Rev. C **99**, 064613 (2019)
50. P.N. de Faria, R. Lichtenthaler, K.C.C. Pires, A.M. Moro, et al., Phys. Rev. C **80**, 004600 (2010)

51. S. Appannababu, R. Lichtenthaler, M.A.G. Alvarez, M. Rodríguez-Gallardo, et al., Phys. Rev. C **99**, 014601 (2019)
52. N.A. Iseri, M. Kamimura, et al., Phys. Rep. **154**, 125 (1987)
53. K.C.C. Pires, R. Lichtenthaler, A. Lepine-Szily, V. Morcelle, Phys. Rev. C **90**, 027605 (2014)
54. N. Keeley, J.M. Cook, K.W. Kemper, et al., Phys. Rev. C **68**, 054601 (2003)
55. A.M. Moro, K. Rusek, J.M. Arias, et al., Phys. Rev. C **75**, 064607 (2007)
56. P.R.S. Gomes, J. Lubian, I. Padron, R.M. Anjos, Phys. Rev. C **71**, 017601 (2005)

Publisher's Note Springer Nature remains neutral with regard to jurisdictional claims in published maps and institutional affiliations.